NJC

ROYAL SOCIETY OF CHEMISTRY

PAPER

View Article Online
View Journal | View Issue

Cite this: *New J. Chem.*, 2020, **44**, 10317

Dinuclear complexes of Mn, Co, Zn and Cd assembled with 1,4-cyclohexanedicarboxylate: synthesis, crystal structures and acetonitrile fluorescence sensing properties†

Luis D. Rosales-Vázquez, [a] Diego Martínez-Otero,[b] Víctor Sánchez-Mendieta, *[b] Jonathan Jaramillo-García,[b] Antonio Téllez-López,[b] Roberto Escudero, [c] Francisco Morales, [c] Josue Valdes-García[a] and Alejandro Dorazco-González *[a]

Received 22nd March 2020,
Accepted 17th May 2020

DOI: 10.1039/d0nj01410a

rsc.li/njc

Four dinuclear complexes: $[Mn_2(H_2O)_2(chdc)_2(bipy)_2]$, **1**; $[Co_2(H_2O)_2(chdc)_2(bipy)_2]\cdot H_2O$, **2**; $[Zn_2(H_2O)_2(chdc)_2(bipy)_2]\cdot H_2O$, **3**; and $[Cd_2(H_2O)_2(chdc)_2(bipy)_2]\cdot H_2O$, **4**; chdc = *e*,*a*-*cis*-1,4,cyclohexanedicarboxylate and bipy = 2,2′-bipyridine, were attained as single crystals under ambient conditions. Crystallographic studies show that complexes **1**, **2** and **3** are isostructural and crystallize in the monoclinic system with the $P2_1/c$ space group. The metal centers in these complexes are hexa-coordinated with a distorted octahedral coordination sphere. Complex **4** crystallizes in the triclinic system with the $P\bar{1}$ space group; in this compound, the metal centers are hepta-coordinated and their coordination sphere is distorted-capped trigonal prismatic. Magnetic property measurements reveal that complexes **1** and **2** exhibit weak antiferromagnetic ordering. Complex **4** displays solid-state blue emission properties and a highly sensitive response to acetonitrile in water based on turn-on fluorescence with a low detection limit of 1.1 μM and selectivity over common polar organic solvents.

1. Introduction

Dinuclear and polynuclear coordination complexes have been synthesized extensively throughout, at least, the past sixty years, primarily as a subject of chemical structure studies and its relationship to properties, such as, magnetism, optics, electronics, *etc.*[1] However, in the last three decades, these types of compounds have been pursued further as functional materials, with novel applications according to their chemical, morphological and textural properties, among others. These applications range from sensing[2] and molecular recognition[3] to catalysis[4] and anticancer.[5] Thus, nowadays, the search for new coordination complexes with fascinating structures but, most importantly, with relevant properties and applications continues to be a hot topic. Among the possible properties that can be incorporated into a coordination compound, luminescence is a very treasured one, since it provides the possibility of using the complex as a fluorescent probe for chemosensing hazardous substances,[6] amid other technological applications. Dinuclear complexes assembled with 1,4-cyclohexanedicarboxylate are, to some extent, rare. To our knowledge, dinuclear complexes of Cu,[7] Mo,[8] Sn,[9] Pb,[10] Eu[11] and Tb[11] have been reported. In most of these complexes the chdc bridging ligand assumes the most common *e*,*a*-*cis* conformation of the carboxylate moieties. The *e*,*e*-*trans* conformation of the chdc ligand is somewhat uncommon, it has been reported only in coordination polymers made with Fe,[12] La,[13] Nd,[14] and Sm[14] and in our work with a 3-D Cd polymer.[15] The rarest conformation is *a*,*a*-*trans*, which has been found only once in a Sm coordination polymer, in combination with the *e*,*e*-*trans* conformation.[16] In most of the literature related to dinuclear complexes using the chdc bridging ligand, structural studies and solid-state fluorescence properties have mainly been investigated, but no further potential applications have been explored.

On the other hand, the development of fluorescent sensors based on d^{10} metal complexes that can detect small-molecule organic solvents with chemical and environmental relevance,

[a] *Instituto de Química, Universidad Nacional Autónoma de México, Circuito Exterior, Ciudad Universitaria, Ciudad de México, 04510, Mexico. E-mail: adg@unam.mx*
[b] *Centro Conjunto de Investigación en Química Sustentable UAEM-UNAM, Carretera Toluca-Ixtlahuaca Km. 14.5, Tlachaloya, Toluca, Estado de México, 50200, Mexico. E-mail: vsanchezm@uaemex.mx*
[c] *Instituto de Investigaciones en Materiales, Universidad Nacional Autónoma de México, Apartado Postal 70-360, Ciudad de México, 04510, Mexico*

† Electronic supplementary information (ESI) available: CCDC 1907858–1907861 (**1**–**4**). For ESI and crystallographic data in CIF or other electronic format see DOI: 10.1039/d0nj01410a

such as DMF, alcohols, aromatic solvents, acetone and CH_3CN, has become an active area in research within supramolecular chemistry and materials science.[17–19] It is well known that the interplay between d^{10} metal centers and organic aromatic ligands such as 2,2′-bipy derivatives with flexible multi-carboxylate acids offers structural diversity and versatile photoluminescence processes.[20–23] In this context, Zn(II)/Cd(II) complexes containing one available coordination site occupied by a labile solvent molecule are potential molecular sensors for coordinating solvents with higher affinity for the metal center, by a solvent exchange reaction.[15]

Herein, we provide the crystallographic and structural studies of four novel dinuclear complexes made up of Mn, Co, Zn and Cd with 1,4-cyclohexanedicarboxylate as a bridging ligand and 2,2′-bipyridine as an ancillary ligand. Magnetic properties of Mn and Co complexes are presented. Moreover, the Zn and Cd complexes exhibit strong blue photoluminescence in the solid state; remarkably, the Cd dinuclear complex is an efficient fluorescence sensor of acetonitrile in water.

2. Experimental section

2.1 Materials and methods

All chemicals were of analytical grade, purchased commercially (Aldrich) and used without further purification. All syntheses were carried out under aerobic and ambient conditions. Elemental analyses for C, H, and N were obtained by standard methods using a Vario Micro-Cube analyzer. IR spectra of the complexes were obtained using a FT-IR Shimadzu spectrophotometer, IR Prestige-21, from 4000 to 500 cm^{-1}. Magnetic characteristics of the complexes were determined using a MPMS Quantum Design magnetometer, with measurements performed at zero field cooling (ZFC) and field cooling (FC) from 2 to 300 K and *vice versa*. The applied magnetic field was 1000 Oe, and diamagnetic corrections were estimated using Pascal's constants as -250×10^{-6} cm^3 mol^{-1}.

2.2 Synthetic procedures

$[Mn_2(H_2O)_2(chdc)_2(bipy)_2]$ (1). Firstly, disodium 1,4-cyclohexanedicarboxylate was prepared by adding an aqueous solution of NaOH (5 ml; 0.16 M) to a methanol solution (5 ml) of 1,4-cyclohexanedicarboxylic acid (0.0688 g; 0.4 mmol). A solution of 2,2′-bipyridine (0.0624 g; 0.4 mmol) in DMF (5 ml) was added to the solution of sodium 1,4-cyclohexanedicarboxylate while stirring. Then, a deionized water solution (25 ml) of $MnCl_2{\cdot}4H_2O$ (0.07916 g; 0.4 mmol) was added. A yellow translucent solution was obtained. After two weeks, yellow crystals formed; these were filtered out and washed with deionized water. Yield: 79% based on the metal precursor. Elemental analysis (%), $C_{36}H_{40}Mn_2N_4O_{10}$, cal.: 54.14% C, 5.05% H, 7.02% N; found: 53.76% C, 5.16% H 7.06% N.

$[Co_2(H_2O)_2(chdc)_2(bipy)_2]{\cdot}H_2O$ (2). Analogous conditions to the synthesis of **1** were used, except that in this case, a solution of 2,2′-bipyridine (0.0624 g; 0.4 mmol) in methanol (5 ml) was added to the solution of sodium 1,4-cyclohexanedicarboxylate while stirring. Then, a deionized water solution (10 ml) of $Co(NO_3)_2{\cdot}6H_2O$ (0.1164 g; 0.4 mmol) was added. A red-brown translucent solution was obtained. After five days, red crystals were deposited; these were filtered out and washed with deionized water. Yield: 73% based on the metal precursor. Elemental analysis (%), $C_{36}H_{44}Co_2N_4O_{12}$, cal.: 51.31% C, 5.26% H, 6.65% N; found: 51.69% C, 5.17% H 6.68% N.

$[Zn_2(H_2O)_2(chdc)_2(bipy)_2]{\cdot}H_2O$ (3). Similar conditions to the synthesis of **1** were used, except that a deionized water solution (25 ml) of $Zn(NO_3)_2{\cdot}6H_2O$ (0.09413 g; 0.4 mmol) was added. After five days, white crystals were deposited; these were filtered out and washed with deionized water. Yield: 79% based on the metal precursor. Elemental analysis (%), $C_{36}H_{44}N_4O_{12}Zn_2$, cal.: 50.54% C, 5.18% H, 6.55% N; found: 50.71% C, 5.10% H, 6.77% N.

$[Cd_2(H_2O)_2(chdc)_2(bipy)_2]{\cdot}H_2O$ (4). Comparable conditions to the synthesis of **1** were used, except that a deionized water solution (10 ml) of $Cd(NO_3)_2{\cdot}4H_2O$ (0.1233 g; 0.4 mmol) was added. After three days, white crystals formed; these were filtered out and washed with deionized water. Yield: 82% based on the metal precursor. Elemental analysis (%), $C_{36}H_{44}Cd_2N_4O_{12}$, cal.: 45.53% C, 4.67% H, 5.90% N; found: 45.44% C, 4.61% H, 5.89% N.

2.3 X-ray crystallography

Crystallographic data for **1–4** were collected using a Bruker APEX II CCD diffractometer, at 100 K, using Mo-Kα radiation (k = 0.71073 Å) from an Incoatec IμS source and Helios optic monochromator.[24] Suitable crystals were coated with hydrocarbon oil (Parabar), picked up with a nylon loop, and mounted in the cold nitrogen stream of the diffractometer. The structures were solved using intrinsic phasing (SHELXT)[25] and refined by full-matrix least-squares on F^2 [25] using the shelXle GUI.[26] The hydrogen atoms of the C–H bonds were placed in idealized positions whereas the hydrogen atoms from water molecules were localized from the difference electron density map, and their position was refined with U_{iso} tied to the parent atom with distance restraints. In compound **4**, the hydrogens from water molecules present positional disorder in two positions, the occupation was set at 50% and their positions were localized from the difference electron density map and refined using DFIX instruction. In compound **4**, one carboxylate moiety presented positional disorder that was solved using SIMU, RIGU and SADI instructions and the occupancy was refined using a free variable.

Crystallographic data for **1–4** have been deposited at the Cambridge Crystallographic Data Center (CCDC) with the numbers 1907858–1907861,† respectively.

The crystallographic data and refinement details for the complexes are summarized in Table S1 (ESI†). Selected bond lengths, angles, and hydrogen bond interactions for **1–4** are listed in Tables S2–S5, respectively, ESI.†

2.4 Photoluminescence properties

Luminescence spectra in the solid state and those of suspensions of **3** and **4** were recorded using a Fluorometer Agilent Cary

Eclipse system equipped with a crystal holder or a thermostated cell holder with a quartz cuvette. In all cases, single crystalline samples of as synthesized **3** and **4** were used. The suspensions of **4** were prepared by stirring for 10 min at 25 °C using spectrophotometric grade solvents and double distilled water with a concentration of 50.0 μM. Luminescence quantum yields were determined using an aqueous solution of quinine sulfate containing H_2SO_4 (0.5 M) as standard (Φ = 0.546; excited at 360 nm). For the determination of the quantum yield, the excitation wavelength was chosen so that $A < 0.05$[27,28] using the following equation: $\Phi_s = \Phi_r(A_rF_s/A_sF_r)(n_s^2/n_r^2)$, where, s and r denote sample and reference, respectively, A is the absorbance, F is the relative integrated fluorescence intensity, and n is the refractive index of the solvent or solvent mixture. The solid state quantum yield was measured according to the procedure reported by Pålsson,[29] using an integrating sphere previously mounted onto a Jobin Yvon Horiba Fluoromax-3 spectrofluorometer.[29]

3. Results and discussion

3.1 Crystal structures

The dinuclear complex **1** consists of two Mn(II) ions, and two aqua, two chdc and two bipy ligands, as shown in Fig. 1. The Mn(II) ions are hexa-coordinated in a distorted octahedral geometry, each coordinated by three carboxyl oxygen atoms of chdc, two nitrogen atoms from bipy and one oxygen atom from the aqua molecule. The Mn–O bond lengths range from 2.0937(10) to 2.2818(10) Å, while the Mn–N distances are 2.2612(12) and 2.2969(12) Å, which are similar values to those reported for related compounds.[30–32]

Compounds **1**, **2** and **3** are isostructural (Fig. 1 and Fig. S1, S2, ESI†). Therefore, only a few differences are emphasized here, such as bond lengths. In **2**, the Co–O bond lengths range from 2.0638(10) to 2.1974(10) Å, while the Co–N distances are 2.0808(12) and 2.1356(12) Å, which are values that are close to the ones reported for related compounds.[33–35] For **3**, the Zn–O bond lengths range from 2.0549(11) to 2.3105(12) Å, and the Zn–N distances are 2.0894(13) and 2.1765(13) Å, which are like those values reported for associated complexes.[36–38] These dinuclear complexes are formed due to the presence of both monodentate and chelate bidentate coordination modes of chdc ligands, and the *equatorial* and *axial cis* configurations of their carboxylate moieties bridging the two metal ions. We have previously found similar coordination modes of this bridging ligand in 1-D Co(II) coordination polymers.[39] It is worthwhile mentioning that by varying the solvent–water mixtures in the synthesis, we have been able to obtain coordination polymers[15] or complexes with the chdc bridging ligand, using CH_3OH or DMF, respectively. Although these findings require more investigation, it seems that depending on the co-solvent used, there are subtle changes in the solubility of the polymeric *vs* dimeric compounds, leading to the crystallization of different products. This opens an alternative route for trying to control the dimensionality of coordination complexes.[40]

The crystal packing of complexes **1**, **2** and **3** is further stabilized by hydrogen bonds. Adjacent complex units of **1** are connected by hydrogen bonds formed between non-coordinated (O2) and coordinated (O3) carboxyl-oxygen atoms of the two chdc and the oxygen (O5) of the coordinated water. This supramolecular assembly leads to a zigzag 1-D array (Fig. 2). Similar to **1**, molecules of **2** and **3** are bridged by hydrogen bonds, including the ones formed by the corresponding crystallization water molecules, creating also zig-zag 1-D chains (Fig. S3 and S4, ESI†).

The dinuclear complex **4** exhibits a distorted-monocapped trigonal prismatic coordination environment in its hepta-coordinated metal centers, coming from two chdc, two bipy and one coordinated water molecule (Fig. 3). Unlike complexes **1–3**, in **4**, the chdc ligand coordination mode is chelate bidentate at both carboxylate groups. The metal to nitrogen distances are 2.3537(13) and 2.3574(13) Å. The metal to oxygen distances for chcd range from 2.3467(11) to 2.580(3) Å. The M–O bond for the coordinated water molecule is 2.3085(11) Å. The reported Cd(II) hepta-coordinated complexes exhibit similar bond length values.[41–43]

Due to the noticeable differences in distances and the corresponding angles that give form to the trapezoid and triangular faces, in the distorted-monocapped trigonal prismatic geometry of Cd(II) in **4**, the two triangular faces are not parallel (Fig. S5, ESI†). Thus, the planes defined by O1–N1–O3 and O5–N2–O4 make an angle of 22.3°, known as the Bailar twist angle.[44] Intermolecular hydrogen-bonding interactions assemble complex **4** into a 2-D supramolecular array. These interactions are promoted by the presence of both the aqua ligand and the crystallization

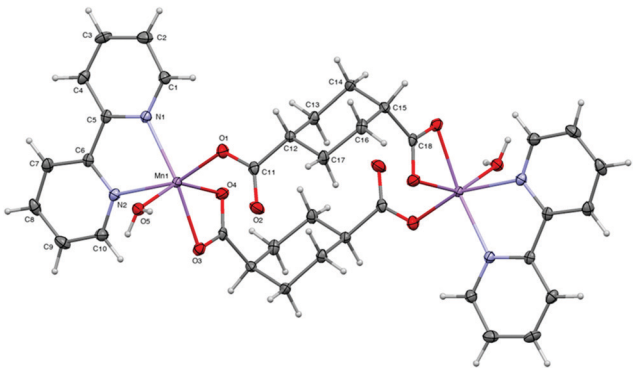

Fig. 1 Molecular structure of **1** (ellipsoids shown at 60% probability).

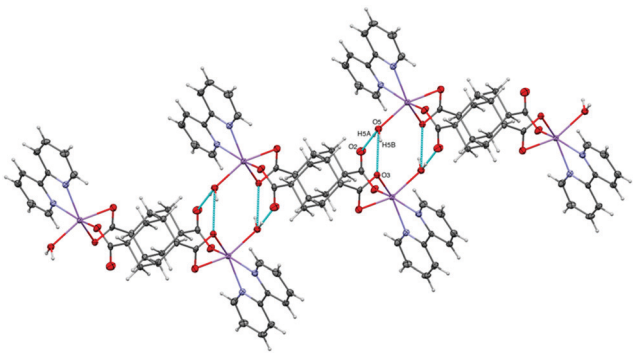

Fig. 2 Supramolecular 1-D zig-zag chain of **1** formed by hydrogen-bonding interactions (ellipsoids shown at 60% probability).

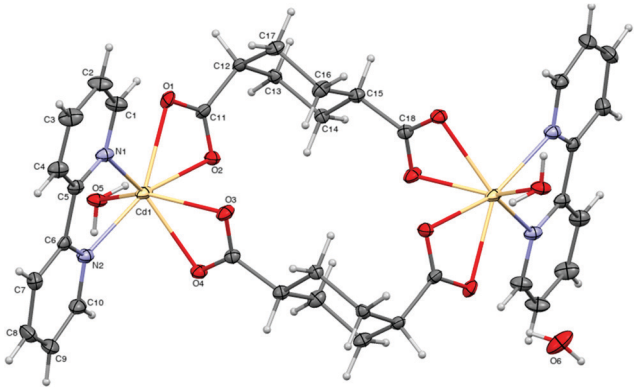

Fig. 3 Molecular structure of **4** (ellipsoids shown at 50% probability).

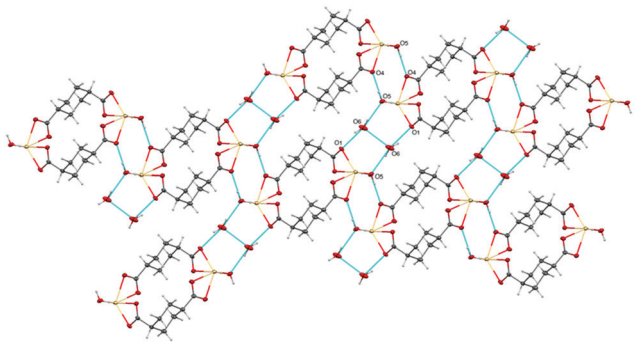

Fig. 4 Supramolecular 2-D array of **4** formed by hydrogen-bonding interactions (chdc ligands are omitted for clarity. Ellipsoids shown at 60% probability).

water molecule. This is shown in Fig. 4, where the main O–H···O interactions involve the O–H moiety (O5) of the aqua ligand with an oxygen atom (O4) of the chdc ligand in an intermolecular hydrogen bond. Furthermore, each water ligand (O5) generates a double hydrogen bridge; the one described above, and another with the oxygen atom (O6) of non-coordinated water, which also forms a hydrogen bond with the oxygen atom (O1) of a neighboring chdc ligand (another intermolecular hydrogen bond), yielding thus the 2-D supramolecular arrangement.

3.2 Magnetic properties of 1 and 2

DC magnetic susceptibility, χ, was determined for **1** and **2**, in zero field cooling (ZFC) and field cooling (FC) modes, from 2–300 K and *vice versa*, in an applied field of 1000 Oe. χT values at room temperature are 13.4 and 5.6 $cm^3\ mol^{-1}$ K for **1** and **2**, respectively, which are higher than the value expected for two magnetically isolated Mn^{2+} (S = 5/2) (8.7 $cm^3\ mol^{-1}$ K) and close to the value of two magnetically isolated Co^{2+} (S = 3/2) (5.2 $cm^3\ mol^{-1}$ K), respectively. Particularly for compound **1**, the χT at 300 K is close to a value when three Mn^{2+} ions would be interacting (~13.0 $cm^3\ mol^{-1}$ K).[45] The calculated magnetic susceptibility (χ_M) *vs.* temperature plots for **1** and **2** can be seen in Fig. 5 and 6, respectively.

Even though no maximum is detected in the magnetic susceptibility plots, the observed increase of χ_M and the decrease in χT (Fig. S6 and S7, ESI†), with decreasing temperature, suggest

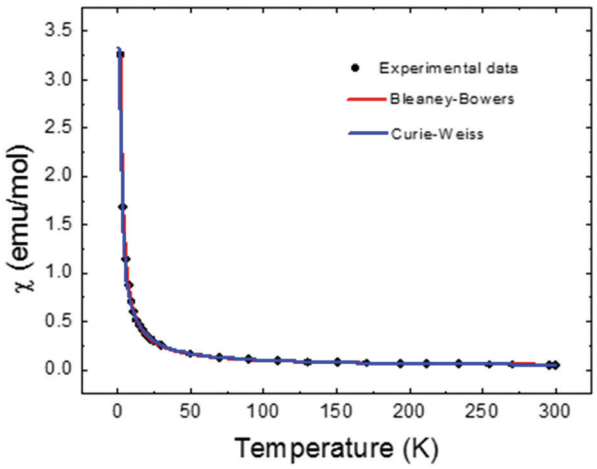

Fig. 5 χ_M *vs.* T plot for **1**.

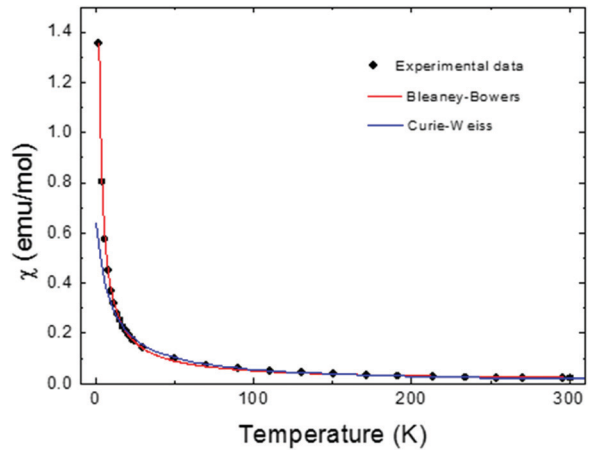

Fig. 6 χ_M *vs.* T plot for **2**.

weak antiferromagnetic coupling in both compounds. Once fitting the obtained data to the Curie–Weiss model:

$$\chi_M = C/(T - \Theta) \quad (1)$$

the Curie constants were determined to be C = 7.4 and 6.0 emu·K mol^{-1} for **1** and **2**, respectively; for S = 5/2 and S = 3/2, respectively, with a small orbital contribution, not totally quenched, which leads to an orbital angular contribution value of less than one. The Curie–Weiss temperatures were determined to be $\Theta_{(C\text{-}W)}$ = −1.93 and −9.45 K for **1** and **2**, respectively, both indicative of a weak antiferromagnetic ordering. Frequently, the effects of spin–orbit coupling occur in combination with the effects of a symmetry-lowering structural distortion, away from O_h symmetry,[46] as in these complexes.

Due to the dinuclear nature of complexes **1** and **2**, and to the difficulty of fitting the Curie–Weiss model to the χ *vs.* T plot, particularly below 25 K for compound **2** (Fig. 6), the experimental data were fit using the Bleaney–Bowers eqn (2)[47] for coupled S = 5/2 and S = 3/2 dimeric units, respectively.

$$\chi = (1-\rho)\frac{N_A g^2 \mu_B{}^2 \left(2e^{2J/k_B T}\right)}{k_B (T-\theta)(1+3e^{2J/k_B T})} + \rho\frac{N_A g^2 \mu_B{}^2}{2k_B T} \quad (2)$$

where Θ is the Curie–Weiss temperature and J is the magnetic spin exchange interaction according to the Hamiltonian interaction: $H = -2J\ (S_1 \cdot S_2)$, between two metal magnetic moments in the dimeric unit. The second term in eqn (2) refers to the noninteracting paramagnetic species, with the factor ρ as the molar fraction of these paramagnetic moments, k_B is the Boltzmann constant, N_A is the Avogadro number and μ_B is the Bohr magneton. The best fit of the experimental data was obtained with $J = 133\ cm^{-1}$, $g = 1.61$, and $\Theta = -0.3$ K for **1**, and $J = 97\ cm^{-1}$, $g = 1.34$, and $\Theta = -2.4$ K for **2**. Thus, even though the g values are low and the J values obtained are higher than expected for both complexes, the small and negative Θ values confirm the weak antiferromagnetic interaction between the metal centers in complexes **1** and **2**, as obtained by the Curie–Weiss approach. It is important to mention that the Bleaney–Bowers model has been applied for other complexes and coordination polymers having similar dinuclear units.[48,49] Attempts to fit the magnetic susceptibility data of **2** to the Rueff phenomenological approach,[50] in order to account for the spin–orbit coupling and the magnetic interaction, resulted in divergence of the refinement. So, the magnetic behavior of **1** and **2** agrees well with a weak antiferromagnetic intramolecular interaction between the metal centers, which has usually been found in the *syn–syn*, equatorial–equatorial arrangement in carboxylate bridges of metal ions in analogous dinuclear units.[51] The magnetic properties obtained are also in good accordance with the M···M distances found in **1** and **2**, because of their structural particularities. Complexes **1** and **2** exhibit the shortest distance between metal centers through their supramolecular structures (5.272 and 6.997 Å, respectively) (Fig. 2 and Fig. S3, ESI†); therefore, they display only weak magnetic interactions. We have found similar magnetic properties in complexes and coordination polymers with analogous structural characteristics, where the metal centers are separated by no more than 5 Å, while magnetic exchange was not found in compounds where the metal ion distances fluctuate from 7 to 10 Å.[52]

3.3 Photoluminescence properties of 3 and 4

In the solid-state, **4** exhibits a photoluminescence emission with a band centered at 370 nm, corresponding to a purplish blue color in the CIE-1931 chromaticity diagram, upon excitation at 290 nm, as shown in Fig. 7. In contrast, crystals of **3** display a modest emission intensity at 360 nm with a shoulder band at 369 nm under the same excitation conditions. The emission broad bands for complexes **3** and **4** can be assigned to effective coordination of the chelating N-aromatic ligands to the Zn(II) and Cd(II) ions with a blue-shift ($\Delta \sim$ 5–15 nm) by comparison to the weak fluorescence intensities and emission maxima of the free bipy (λ_{em} = 375 nm, and λ_{ex} = 290 nm) and chdc (λ_{em} = 339 and 431 nm, and λ_{ex} = 290 nm) ligands.[17,53] It is well known that increased fluorescence emission of bipy derivatives on complexation with d^{10} transition metals is due to the increase of the rigidity of the aromatic heterocyclic ligand in the final crystal arrangement, which reduces the loss of energy through non-radiative processes.[54–59] Typically, the emission located in the range of 380–440 nm for free aromatic N-donors is assigned to the intraligand charge transitions (ICTs) entailing the filled π(HOMO) and empty π*(LUMO) orbitals.[57,60,61]

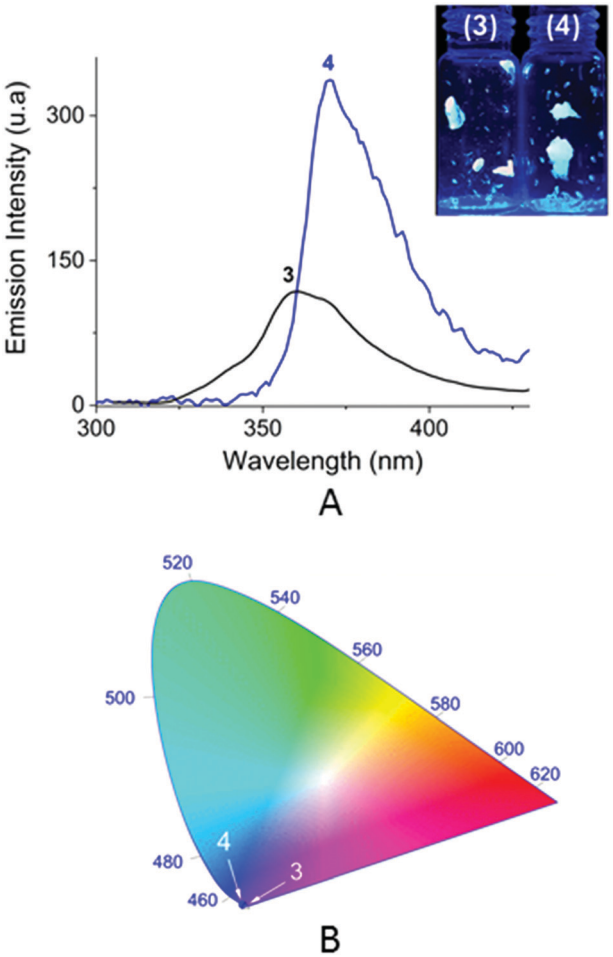

Fig. 7 (A) Solid-state emission spectra (λ_{ex} = 290 nm) of **3** and **4** at room temperature. The inset shows the photographs of crystals of **3** and **4** under UV light of 365 nm. (B) The corresponding color coordinate diagram of emission.

The photoluminescence quantum yield of **4** in the solid state is $\Phi_{ss} = 0.1$ at room temperature. Similar quantum efficiencies (<0.4) have been observed for a series of Cu(I) complexes bearing bipyridines in the solid state and these have been assigned to a ligand-to-metal charge transfer (LMCT)-excited state involving the coordinated bipy.[62]

We have reported previously several dinuclear Zn(II)/Cd(II) polymeric structures bearing di-alkyl-bipy ligands with emission bands in the range of 370–440 nm.[15,28,63] Furthermore, similar photophysical properties for several Zn(II)/Cd(II) polynuclear complexes and metal organic frameworks containing [*N*,*N*]-chelating ligands, such as 2,2′-bipy derivatives and multicarboxylate or arenesulfonate anions, have been reported; for recent examples, see: $[Cd_2(L^1)_2(2,2'\text{-bipy})_2]$,[20] $\{[Cd_5(L^2)_2(2,2'\text{-bipy})_4(H_2O)_4]\text{-bpy}\cdot(NO_3)_2\cdot(H_2O)_8\}_n$,[18,53] $\{[Zn_2(L^3)(2,2'\text{-bipy})(H_2O)_2]\cdot 3H_2O\}_n$.[59,64] $\{[Zn_3(2,2'\text{-bipy})_2(L^4)_2\ (H_2O)_2]\cdot 4H_2O\}_n$,60[56,65] $[Cd_2(\textit{trans}\text{-chdc})(\textit{cis}\text{-chdc})(2,2'\text{-bpp})_2]_n$,[22,53] and $[Cd_{1.5}(L^5)(2,2'\text{-bipy})]$, where: L^1 = 2-hydroxy-5-chloro-1,3-benzenedisulfonic acid, L^2 = (ethylene-bis(oxyethylenenitrilo) tetraacetic acid), L^3 = 4-((3,5-dicarboxyphenyl)carbamoyl)phthalic acid, L^4 = 1*H*-1,2,3-triazole-4,5-dicarboxylic acid, bpp = (1,3-bis(4-pyridyl)propane) and

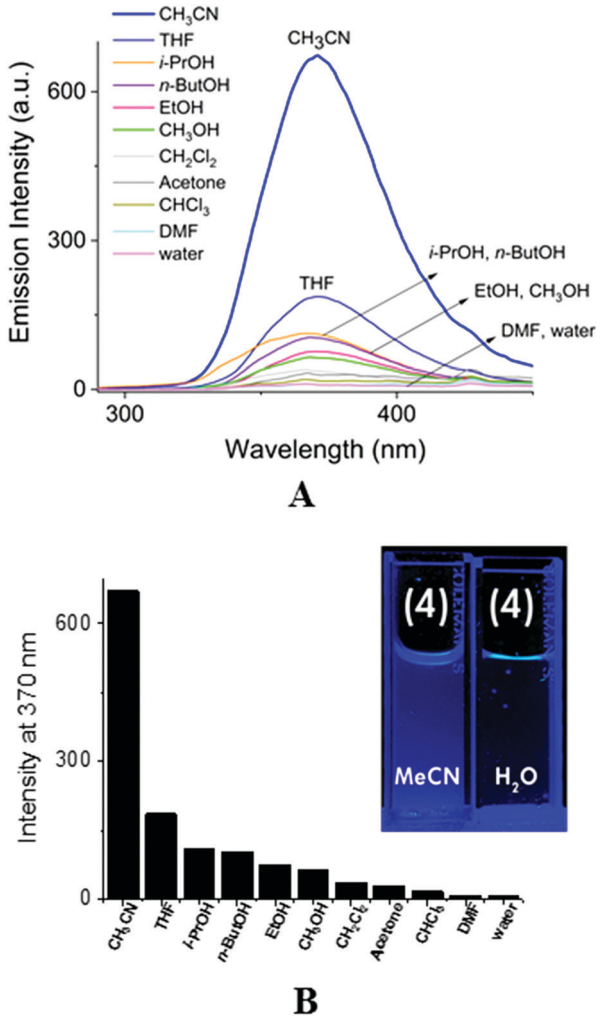

Fig. 8 (A) Emission spectra of **4** (50 μM) dispersed in different organic solvents and water. (B) Fluorescence intensity ratio histograms of **4** in different solvents. The inset shows acetonitrile and water suspensions of **4** under irradiation of 365 nm UV-light.

L^5 = 3-(2′,3′-dicarboxylphenoxy) benzoic acid. The photoluminescence of these kinds of d^{10} metal complexes is assigned to ligand-to-metal charge transfer (LMCT)[17,61] in combination with perturbed π–π and π–n* transitions.[22,57]

To explore the potential sensing properties of **4**, photoluminescence spectra of its liquid suspensions in several pure organic solvents and water were measured. Fig. 8 shows the family of spectra (λ_{ex} = 290 nm) of **4** (~50 μM). In general, the emission intensity is strongly dependent on the solvent molecules. Specifically, in the case of acetonitrile and water, it displayed the highest emission intensity and the most significant quenching effect, respectively (Fig. 10B).

All alcohols (CH_3OH, EtOH, i-PrOH, and *n*-ButOH), chlorinated solvents and THF showed a modest but significantly lower emission than that observed for acetonitrile. In contrast, suspensions in DMF, acetone and water practically do not present photoluminescence. Particularly in water, this fact is not unexpected, because water molecules in the first coordination sphere are among the most efficient vibrational quenchers.[17] Taking the above results and the chemical, environmental and industrial relevance of acetonitrile into account,[66] we used a pure aqueous suspension to sense this solvent by "turn-on" fluorescence. As mentioned before, compound **3** emits weaker light compared to **4**, and for this reason, only the photoluminescence sensing properties of **4** were studied, and this fact may be ascribed to the presence of the dinuclear core, [{Cd(1)N_2O_5}^{Cd(2)N_2O_5}], involving multiple μ-CO_2 ligands, which may rigidify the whole cluster, thus resulting in much weaker vibrations.[58] Nowadays, most luminescent transition-metal-based sensors used for quantification of volatile organic solvents operate under quenching processes and, interestingly, the literature features very few examples for the optical sensing of acetonitrile.[17,67,68]

Next, a fluorescence titration experiment was carried out by addition of increasing amounts of CH_3CN to a suspension of **4** (50 μM) in pure water, as shown in Fig. 9. Notably, there was a linear dependence of the fluorescence intensity on the acetonitrile concentration in the range of 0–0.8 mM (R^2 = 0.993) with a detection limit of 1.1×10^{-6} M. The detection limit is defined as LOD = $3\sigma/s$, where σ is the standard deviation of the blank and s is the slope of the calibration curve (s = 9.06(±0.08) × 10^5). The enhancement of the photoluminescence intensity upon the addition of acetonitrile (I_F/I_o = 67) could be attributed to a dehydration process through an efficient dynamic exchange of coordinated water molecules by acetonitrile molecules. Reversible water-exchange by polar organic solvents has been reported recently for metal-based luminescent sensors.[15,17,69]

We further examined the quantum fluorescence yield (Φ) of **4** in mixtures of water–acetonitrile with different ratios (25%, 50% and 75%, v/v) and pure acetonitrile at room temperature. The quantum yields in these solvent mixtures ($\Phi_{25\%}$ = 0.035, $\Phi_{50\%}$ = 0.048, and $\Phi_{75\%}$ = 0.062) increased depending on the concentration of CH_3CN up to a maximum value of Φ_{CH_3CN} = 0.083 in acetonitrile. This enhanced quantum yield may result from the decreased hydration,[17] both in the number of the

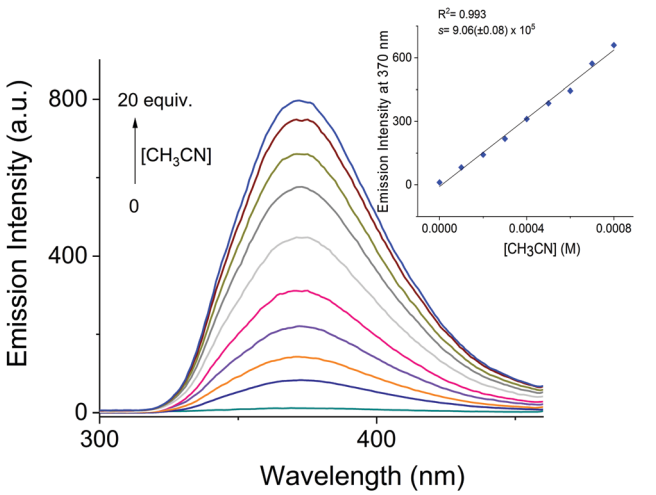

Fig. 9 Changes of the emission spectra (λ_{ex} = 290 nm) of a pure aqueous suspension of **4** upon addition of increasing amounts of CH_3CN (0–0.8 mM). The inset shows the calibration curve with a linear fit at λ_{em} = 370 nm.

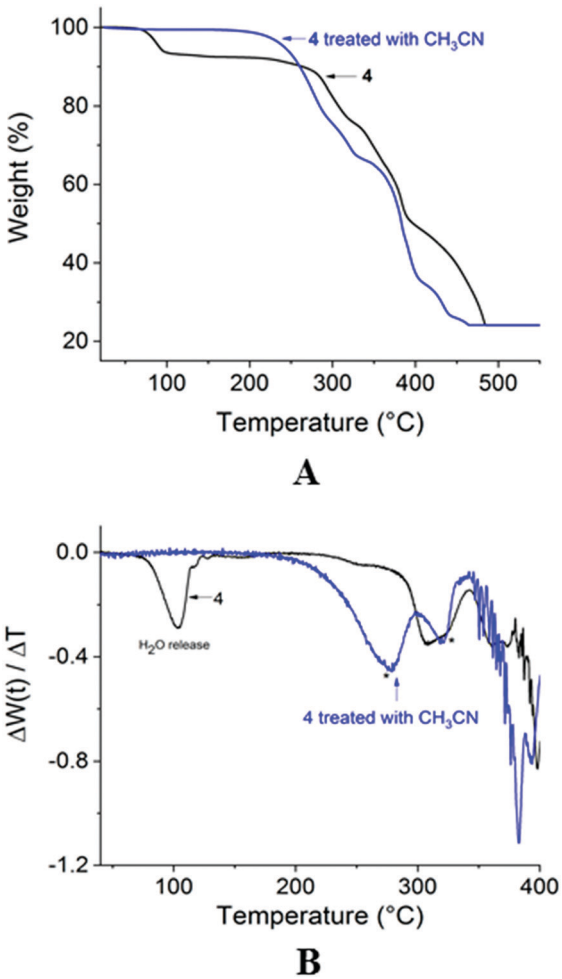

Fig. 10 (A) TGA of the aqua complex **4** (black) and after treatment with CH_3CN by stirring at r.t. (blue). (B) First-derivative TGA plots of solvent exchange. * Decomposition of the complexes.

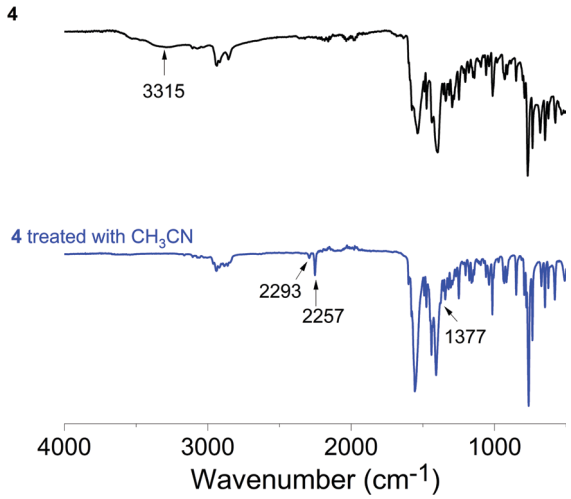

Fig. 11 FT-IR spectra of **4** before (black) and after treatment with CH_3CN (blue).

coordinated water molecules and the crystallization water molecules, with a possible contribution of the aggregation-induced emission (AIE) mechanism.[70]

In order to confirm this solvent-exchange with fluorescence enhancement in **4**, thermogravimetric analysis (TGA) and FT-spectra of aqua complex **4** and a sample of this dinuclear complex treated with CH_3CN, by stirring at r.t., filtering and drying under vacuum, were measured and compared. The TGA curve of **4** (Fig. 10A) shows a continuous weight loss of 7.47% from 80 to 130 °C, corresponding to the removal of two crystallization water molecules and two coordinated water molecules (calcd 7.58%), and no further mass loss was observed until 220 °C. The decomposition process of **4** was observed up to 280 °C. In contrast, the treated dinuclear Cd(II) complex with acetonitrile, shows a different thermal curve with a loss of mass of 40% at a higher temperature range of 170–337 °C in comparison with that observed in the aqua complex **4**, which can be ascribed to the removal of two CH_3CN molecules and two bypi ligands (calcd 41.1%). Finally, the FTIR spectrum of the treated sample **4** (Fig. 11) shows typical bands (cm^{-1}) for CH_3CN at 2293 (stretch, CH_3), 2257 (stretch, CN) and 1377 (*s*-deformation, CH_3) and the characteristic water band at 3315 cm^{-1} was not observed. This fact clearly supports a dynamic solvent-exchange and it is consistent with the IR spectra. For practical applications, sensors are required to have not only a good optical response and affinity but also recyclability. Thus, we studied the reversibility of this water–CH_3CN exchange and the successive fluorescence sensing ability for acetonitrile, considering that it can be easily monitored by IR spectroscopy. Complex **4** can be straightforwardly reactivated by heat desolvation (~70 °C) under vacuum for 2 h with subsequent hydration and reused for four cycles of CH_3CN detection–activation without the loss of sensing ability and retaining the original intensity (~84%), as shown in Fig. S8 (ESI†). Overall, these results highlight the potential utility of simple cadmium-based complexes for efficient sensing of small-molecule solvents.

4. Conclusions

Four dinuclear complexes of Mn (**1**), Co (**2**), Zn (**3**) and Cd (**4**) were obtained under ambient conditions, using 1,4-cyclohexanedicarboxylate and 2,2′-bipyridine as bridging and ancillary ligands, respectively. Complexes **1–3** are isostructural with a pseudo-octahedral coordination sphere and 1D supramolecular assembly formed by hydrogen bonding. Complex **4** exhibits an unusual distorted capped trigonal prismatic coordination sphere, with a 2D supramolecular array formed *via* hydrogen bonding. Complexes **1** and **2** show very weak antiferromagnetic coupling according to Curie–Weiss law fitting. Complex **3** displays only moderate blue photoluminescence emission, unlike complex **4**, which exhibits very strong blue photoluminescence emission in the solid state and is capable of sensing acetonitrile selectively and reversibly in water with the very low detection limit of 1.1×10^{-6} M, and selectivity over alcohols, acetone and DMF. The outstanding sensing ability of **4** for acetonitrile, in combination with its high-yielding synthesis and photophysical properties, makes it a promising candidate for the design of more sophisticated materials with application in the sensing of small molecule solvents.

Conflicts of interest

There are no conflicts to declare.

Acknowledgements

The authors are thankful to M. en C. Alejandra Nuñez Pineda and L. I. A. María Citlalit Martínez Soto (CCIQS UAEM-UNAM) for elemental analysis and computing assistance, respectively. Funding for this work was provided by the Universidad Autónoma del Estado de México (project 4995/2020CIB). We thank UNAM (PAPIIT-UNAM IN216220) and CONACyT for PhD scholarships 713164 and 848787 to L. D. R.-V. and J. V.-G, respectively. R. Escudero acknowledges DGAPA-UNAM, project 1T100217; the authors thank M. C. Ana Bobadilla for the liquid He, Carlos Reyes Damian for technical support, A. López and A. Pompa-Garcia for help with the graphs and figures.

Notes and references

1 E. Berti, A. Caneschi, C. Daiguebonne, P. Dapporto, M. Formica, V. Fusi, L. Giorgi, A. Guerri, M. Micheloni, P. Paoli, R. Pontellini and P. Rossi, *Inorg. Chem.*, 2003, **42**(2), 348.
2 G. Li, D. Zhu, X. Wang, Z. Su and M. R. Bryce, *Chem. Soc. Rev.*, 2020, **49**, 765.
3 M. M. Rhaman, M. H. Hasan, A. Alamgir, L. Xu, D. R. Powell, B. M. Wong, R. Tandon and M. A. Hossain, *Sci. Rep.*, 2018, **8**, 286.
4 A. E. Martell, J. Perutka and D. Kong, *Coord. Chem. Rev.*, 2001, **216–217**, 55.
5 R. W.-Y. Sun, M. Zhang, D. Li, Z.-F. Zhang, H. Cai, M. Li, Y.-J. Xian, S. W. Ng and A. S.-T. Wong, *Chem. – Eur. J.*, 2015, **21**, 18534.
6 N. Kwon, Y. Hu and J. Yoon, *ACS Omega*, 2018, **3**(10), 13731.
7 V. F. Shul'gin, Y. V. Trush, O. V. Konnik, E. B. Rusanov, V. Y. Zub and V. V. Minin, *Russ. J. Inorg. Chem.*, 2011, **56**(5), 707.
8 S. Takamizawa, W. Moil, M. Furihata, S. Takeda and K. Yamaguchi, *Inorg. Chim. Acta*, 1998, **283**, 268.
9 C. Ma, Y. Wang and R. Zhang, *Inorg. Chim. Acta*, 2009, **362**, 4137.
10 J. Yang, J.-F. Ma, Y.-Y. Liu, J.-C. Ma and S. R. Batten, *Cryst Growth Des*, 2009, **9**(4), 1894.
11 L.-N. Dong, Y. Tian, X. Li and Y. Jiang, *J. Coord. Chem.*, 2010, **63**(12), 2088.
12 Y.-Z. Zheng, W. Xue, W.-X. Zhang, M.-L. Tong, X.-M. Chen, F. Grandjean, G. J. Long, S.-W. Ng, P. Panissod and M. Drillon, *Inorg. Chem.*, 2009, **48**, 2028.
13 G. Tian, G. Zhu, B.-L. Su and S. Qiu, *J. Mater. Sci.*, 2009, **44**, 6576.
14 J. Lü, W.-H. Bi, F.-X. Xiao, S. R. Batten and R. Cao, *Chem. – Asian J.*, 2008, **3**, 542.
15 L. D. Rosales-Vázquez, V. Sánchez-Mendieta, A. Dorazco-González, D. Martínez-Otero, I. García-Orozco, R. A. Morales-Luckie, J. Jaramillo-García and A. Téllez-López, *Dalton Trans.*, 2017, **46**, 12516.
16 J. Lü, W.-H. Bi and R. Cao, *CrystEngComm*, 2009, **11**, 2248.
17 J. Heine and K. Müller-Buschbaum, *Chem. Soc. Rev.*, 2013, **42**, 9232.
18 X.-N. Li, L. Li, H.-Y. Wang, C. Fu, J.-W. Fu, Y.-N. Sun and H. Zhang, *Dalton Trans.*, 2019, **48**, 6558.
19 F. Klongdee, S. Youngme and J. A. Boonmak, *Polyhedron*, 2020, **180**, 114437.
20 Y.-Z. Yu, Y.-N. Li, Z.-D. Deng, Z.-B. Zhu and S. Gao, *Polyhedron*, 2015, **90**, 77.
21 G. Yuan, K.-Z. Shao, D.-Y. Du, X.-L. Wang and Z.-M. Su, *Solid State Sci.*, 2011, **13**, 1083.
22 X.-D. Zhu, Y. Li, W.-X. Zhou, R.-M. Liu, Y.-J. Ding, J. Lu and D. M. Proserpio, *CrystEngComm*, 2016, **18**, 4530.
23 S. Zhang, W. Shi and O. Cheng, *Coord. Chem. Rev.*, 2017, **352**, 108.
24 *APEX 2 software suite*. Bruker AXS Inc., Madison, Wisconsin, USA.
25 G. M. Sheldrick, *Acta Crystallogr.*, 2015, **A71**, 3.
26 C. B. Hübschle, G. M. Sheldrick and B. Dittrich, shelXle, *Appl. Cryst.*, 2011, **44**, 1281.
27 W. A. A. Arafa, M. D. Kärkäs, B.-L. Lee, T. Åkermark, R.-Z. Liao, H.-M. Berends, J. Messinger, P. E. M. Siegbahn and B. Åkermark, *Phys. Chem. Chem. Phys.*, 2014, **16**, 11950.
28 A. Dorazco-González, *Organometallics*, 2014, **33**, 868.
29 L.-O. Pålsson and A. P. Monkman, *Adv. Mater.*, 2002, **14**, 757.
30 A. Koval, M. Huisman, A. F. Stassen, P. Gamez, M. Lutz, A. L. Spek, D. Pursche, B. Krebs and J. Reedijk, *Inorg. Chim. Acta*, 2004, **357**, 294.
31 X. Jiang, H. Liu, B. Zheng and J. Zhang, *Dalton Trans.*, 2009, 8714.
32 N. Kotsakis, C. P. Raptopoulou, V. Tangoulis, A. Terzis, J. Giapintzakis, T. Jakusch, T. Kiss and A. Salifoglou, *Inorg. Chem.*, 2003, **42**(1), 22.
33 M. Tabatabaeea, B.-M. Kukovec and V. Razavimahmoudabadia, *Z. Naturforsch.*, 2011, **66b**, 813.
34 M. Bera, A. B. S. Curtiss, G. T. Musie and D. R. Powell, *Inorg. Chem.*, 2012, **51**(22), 12093.
35 X.-M. Chen, Y.-X. Tong and T. C. W. Mak, *Inorg. Chem.*, 1994, **33**(20), 4586.
36 K. Naskar, S. Maity, S. Jana, B. Dutta, S. Tanaka, D. Mallick, T. Akitsu and C. Sinha, *Cryst. Growth Des.*, 2018, **18**(5), 2986.
37 S.-Q. Zhang, F.-L. Jiang, M.-Y. Wu, J. Ma, Y. Bu and M.-C. Hong, *Cryst. Growth Des.*, 2012, **12**(3), 1452.
38 N. Dutta, A. Majumder, A. Das, A. Chatterjee, M. Tarafder, B. Datta and M. Bera, *J. Mol. Struct.*, 2020, **1206**, 127708.
39 L. D. Rosales-Vázquez, V. Sánchez-Mendieta, I. García-Orozco, S. Hernández-López, D. Martínez-Otero, R. A. Morales-Luckie, R. Escudero and F. Morales, *Inorg. Chim. Acta*, 2018, **471**, 674.
40 R. Seetharaj, P. V. Vandana, P. Arya and S. Mathew, *Arabian J. Chem.*, 2019, **12**, 295.
41 F.-Y. Ge, X. Ma, D.-D. Guo, L.-N. Zhu, Z.-P. Deng, L.-H. Huo and S. Gao, *Cryst. Growth Des.*, 2017, **17**(5), 2667.
42 S. Banerjee, P.-G. Lassahn, C. Janiak and A. Ghosh, *Polyhedron*, 2005, **24**, 2963.
43 J. Granifo, S. Suarez and R. Baggio, *Acta Crystallogr.*, 2015, **E71**, 890.

44 S. Alvarez, *Chem. Rev.*, 2015, **115**, 13447.
45 S. G. Baca, Y. Sevryugina, R. Clérac, I. Malaestean, N. Gerbeleu and M. A. Petrukhina, *Inorg. Chem. Commun.*, 2005, **8**, 474.
46 O. Kahn, *Molecular Magnetism*, VCH Publishers, New York, 1993.
47 B. Bleaney and K. D. Bowers, *Proc. R. Soc. London, Ser. A*, 1952, **214**, 451.
48 S. K. Dey, M. Hazra, L. K. Thompson and A. Patra, *Inorg. Chim. Acta*, 2016, **443**, 224.
49 Y. Lou, J. Wang, Y. Tao, J. Chen, A. Mishimab and M. Ohba, *Dalton Trans.*, 2014, **43**, 8508.
50 J. M. Rueff, N. Masciocchi, P. Rabu, A. Sironi and A. Skoulios, *Eur. J. Inorg. Chem.*, 2001, 2843.
51 C. C. Wang, F. Gao, X. X. Guo, H.-P. Jing, P. Wang and S. J. Gao, *Transition Met. Chem. (N. Y.)*, 2016, **41**, 375.
52 A. Téllez-López, V. Sánchez-Mendieta, J. Jaramillo-García, L. D. Rosales-Vázquez, I. García-Orozco, R. A. Morales-Luckie, R. Escudero and F. Morales-Leal, *Transition Met. Chem. (N. Y.)*, 2016, **41**, 879.
53 R. Gaur, *Inorg. Chem. Front.*, 2019, **6**, 278.
54 T. Lu, J.-Y. Wang, D. Tu, Z.-N. Chen, X.-T. Chen and Z.-L. Xue, *Inorg. Chem.*, 2018, **57**, 13618.
55 Y. Ren, S. Zhou, Z. Wang, M. Zhang, J. Wang and J. Cao, *J. Mol. Struct.*, 2017, **1147**, 292.
56 L.-Y. Zhang, J.-P. Zhang, Y.-Y. Lin and X. M. Chen, *Cryst. Growth Des.*, 2006, **6**, 1684.
57 X. Wang, C. Qin, E. Wang, Y. Li, N. Hao, C. Hu and L. Xu, *Inorg. Chem.*, 2004, **43**, 1850.
58 J. Tao, M.-L. Tong, J.-X. Shi, X.-M. Chen and S.-W. Ng, *Chem. Commun.*, 2000, 2043.
59 P. Suresh and G. Prabusankar, *J. Chem. Sci.*, 2014, **126**, 1409.
60 X.-D. Zhu, Y. Li, W.-X. Zhou, R.-M. Liu, Y.-J. Ding, J. Lü and D.-M. Proserpio, *CrystEngComm*, 2016, **18**, 4530.
61 L. Ma, N. Yu, S. Chen and H. Deng, *CrystEngComm*, 2013, **15**, 1352.
62 L. D. Rosales-Vázquez, J. Valdes-García, I. J. Bazany-Rodríguez, J. M. Germán-Acacio, D. Martínez-Otero, A. R. Vilchis-Néstor, R. Morales-Luckie, V. Sánchez-Mendieta and A. Dorazco-González, *Dalton Trans.*, 2019, **48**, 12407.
63 J. C. Rendón-Balboa, L. Villanueva-Sánchez, L. D. Rosales-Vázquez, J. Valdes-García, A. R. Vilchis-Nestor, D. Martínez-Otero, S. Martínez-Vargas and A. Dorazco-González, *Inorg. Chim. Acta*, 2018, **483**, 235.
64 X.-J. Deng, W. Gu, X. Liu, H.-D. Ju, H.-X. He, B.-L. Wang and Z.-H. Weng, *J. Mol. Struct.*, 2020, **1202**, 127212.
65 G. Yuan, K.-Z. Shao, D.-Y. Du, X.-L. Wang and Z.-M. Su, *Solid State Sci.*, 2011, **13**, 1083.
66 X. Yang, S. Wang, G. Li, F. Zhao, Z. Feng, X. Chen, Z. Zhu, Y. Wang and J. Gao, *Ind. Eng. Chem. Res.*, 2020, **59**(11), 5047.
67 J.-L. Du, X. Lu, T.-L. Shen, C.-P. Li, Y.-J. Mu and L.-J. Li, *Mater. Lett.*, 2015, **158**, 225.
68 J.-M. Zhou, W. Shi, N. Xu and P. Cheng, *Inorg. Chem.*, 2013, **52**, 8082.
69 J.-H. Wang, M. Li and D. Li, *Chem. Sci.*, 2013, **4**, 1793.
70 X. Li, Y. Sun, J. Chen, Z. Wu, P. Cheng, Q. Li, J. Fang and D. Chen, *Polym. Chem.*, 2019, **10**, 1575.